Strength of Brillouin spectroscopy to identify spatial densification model in indented silica

Alice Berthelot, Elodie Romeo, Xavier Dagany, Thierry Deschamps, Eliot Herry, Robin Kineider, Yannis De Leon, Emmeline Brassac, Guillaume Kermouche, Etienne Barthel, et al.

Strength of Brillouin spectroscopy to identify spatial densification model in indented silica .

Alice Berthelot[a,*], Elodie Romeo[a], Xavier Dagany[a], Thierry Deschamps[a], Eliot Herry[a], Robin Kineider[a], Yannis De Leon[a], Emmeline Brassac[a], Guillaume Kermouche[b], Etienne Barthel[c], Christine Martinet[a,*]

[a] *Institut Lumiere Matiere CNRS UMR 5306 Universite Claude Bernard Campus de La DOUA 69622 Villeurbanne*
[b] *Mines Saint-Etienne CNRS UMR 5307 LGF Centre SMS 42023 Saint-Etienne France*
[c] *Laboratoire Sciences et Ingenierie de la Matiere Molle ESPCI Paris PSL University Sorbonne Universite CNRS 75005 Paris France*

Abstract

The aim of this work is to analyse and understand the densification process of silica glasses at the micrometer scale under micro-indentation. At the mesoscopic scale, silica glass, with a very low Poisson's ratio, exhibits a high maximum density change, up to 21% and a very low shear flow under shear stress, in contrast to normal glasses such as float glass, which have a low densification change and a high shear flow under non-isotropic compression. In the case of silica glass, it is observed that the evolution of the densification in the lateral dimension is gradual, as for high Poisson's ratio glasses. However, we find that along the central axis, the evolution with depth is quite different : it presents two regions. In the area immediately below the indenter, the densification is high and almost constant. Just under this imprint, there is a relatively sharp transition to the purely elastic region. Our present study, based on Brillouin diffusion measurements, allows us to improve the description of the imprint for normal/anomalous glass and to explain the localisation of cracks in the silica imprint : in this strained transition zone between these two densified and undensified regions.

Keywords: mechanical of glass, vibrationnal spectroscopies, plasticity, indentation

1. Introduction

1.1. States of Art

Due to its amorphous nature, mechanical transformations of glass, especially plastic deformation, are very difficult to model. The need to predict the response of glass answer to external strains implies the development of closely related experiments and simulations. One model experiment is the study of glasses

∗. Corresponding author
Email addresses: alice.berthelot@univ-lyon1.fr (Alice Berthelot), Christine.martinet@univ-lyon1.fr (Christine Martinet)

under micro-indentation, in particular the analysis of the imprint and the cracks formed during the process, which is strongly dependent on the nature of the glass as described by Rouxel et al [1]. A complementary experiment is the application of pure hydrostatic pressure into the glass sample, where plastic deformation of silicate glasses occurs above the elastic limit, between 6 and 9 GPa, depending on the silicate glass composition [2–7]. For hydrostatic and non-hydrostatic stresses, densification rate depends on the initial structure but also on the thermo-mechanical history and the chemical composition of the glass [8,9]. In particular, non-isotropic stress can induce another plastic deformation process in competition with densification : shear flow [10–12]. Models attempt to determine the effects of each process on the evolution of the glass structure and the emergence of cracks.

In silicate glasses, plastic deformation usually results in a permanent increase in density [13] which has been well correlated with Poisson's ratio by AFM measurements [14]. As an anomalous glass with low Poisson's ratio, fused silica, is more sensitive to densification process than to shear flow. This material has a high capacity for permanent densification up to a density increase of 21 % [15,16]. Soda-lime silicates, with a higher Poisson's ratio and a lower ability to densify compared to silica, are considered as normal glasses and show large plastic shear flows [17]. The plastic behavior of silicate glasses can be described by a hybrid law involving pressure and shear stress [11,18].

1.2. Classical Raman Spectrometry for indents study

In order to validate these indentation models, micro-spectroscopic studies were carried out on indent. To this end, the first measurements have allowed to highlight the normal/anomalous characteristics of different silicate glasses [19]. Micro-Raman spectroscopy studies were then carried out to probe the densification inside the imprint. For the float glass with higher Poisson's ratio, the Raman mapping of the barycentre of the Raman bands 500-700 cm^{-1}, gave a density cartography [6]. Deschamps et al observed a progressive evolution of densification as a function of the distance from the centre of the imprint. The fracture lines that separate the different iso-density regions are well reproduced by finite element simulations [20].

Then, for silica with a low Poisson's ratio, such as pure silica, cartographies of the Raman shift of the D2 band, which corresponds to the breathing mode of 3-fold rings, gave an indentation-induced densification map, which allowed the mechanical behaviour of glasse under indentation to be implemented [21]. For this last experiment, a constitutive law derived from finite element simulations reproduced quite well the experimental results of the indentation-induced densification rate map [11] by also taking into account the hydrostatic hardening behaviour [22]. However, we have recently shown that the D2 band is not only sensitive to densification but also to shear stress and is not a reliable marker of the densification process [23].

Chemical dissolution experiments on silicate imprints after 10mN and 50mN indentations for silica and soda-lime glasses, have allowed the observation of a quasi-homogeneously densified region just below the surface in the indented region [24]. Very recent work of Bruns et al presents results from a classical Raman study of indented pristine silica with loads varying from 0.3 N to 10 N [25]. They study the densification process using Raman spectroscopy of the main band (250 cm^{-1}-550 cm^{-1}) which provides an average analysis of the Si-O-Si angle distribution in glasses and has so far been a good probe of the densification process for hydrostatic compression [26]. By measuring the evolution of the main band centroid with the depth of laser focus, Bruns et al have compared their experimental results with a constitutive finite element analysis. They found that the saturation of densification under indentation is closed to 18 % for different size of indent. Nevertheless, this classical Raman analysis spectrum is problematic if we want to study the spatial evolution of densification. The shape of the laser beam used for Raman spectrometry does not allow to remove the answer of the pristine silica that is located below the indented area. In fact, since the main bands of the Raman spectra of the two glasses (densified and non-densified) overlap strongly, it is difficult to separate the imprint contribution from the far field non-densified response.

1.3. Brillouin Spectrometry for indents study

As an alternative technique to classical Raman spectroscopy, Brillouin scattering spectroscopy can measure the energy of acoustic phonons of transparent materials and provides elastic constants if density, longitudinal and transverse acoustic modes have been measured. The evolution of these coupled physical quantities can then be studied by measuring the Brillouin shift. In the back-scattering geometry, only the longitudinal acoustic mode is measured and Brillouin shift ν_B can be described by the following formula :

$$\nu_B = \frac{2nV_{AL}}{\lambda}$$

where n is the optical refactive index, λ the wavelength of the laser,V_{AL} the longitudinal acoustic wave velocity. V_{AL} depends on Young's modulus, density, Poisson's ratio and the optical refractive index which is difficult to measure. A calibration curve relating the Brillouin shift to the densification factor was then deduced experimentally from macroscopic densified silica samples where the density has been measured by the Archimedian method [27]. Using Brillouin spectrometry, Tran et al studied the densification of the imprint of float glass under 20 N load indentation [7]. Although the Brillouin shift between the indent center and pristine float glass is small, this work has shown that the evolution of the densification rate is progressive within the imprint. Despite the fact that these calibration curves do not take into account the effects of shear

stresses, which are far from negligible in an indentation, this technique is very promising to complement other spectroscopic techniques, as Raman and luminescence spectroscopies [21] and will allow to roughly estimate the density evolution of glass inside the imprints for silicate glasses. Then, our present work proposes to compare the well-known behaviour of a normal silicate glass, float glass, with an anomalous glass, silica, under indentation and to analyse the indented volume by micro-Brillouin spectrometry.

2. Experiments

2.1. Samples description

Samples used in this study correspond to pure SiO_2 glass (commercial "Suprasil 300"), with a low OH content, less than 1 ppm, and a commercial float glass (mainly chemical components : 72% SiO_2, 15% Na_2O, 8% CaO, 4% MgO and about 1% (Al_2O_3 + FeO_3 + SO_3) in mole %). On flat and polished face of these two glasses, Vickers micro-indentations of different loads have been performed from 1 N to 10 N. 1 N load imprints does not exhibit any microscopic fracture initiation whereas 3 N and 10 N load imprints show microscopic fractures below the indent and laterally close to the surface of the glass.

2.2. Brillouin spectrometric measurements

We performed micro-Brillouin experiments at room temperature, using a Sandercock tandem Fabry Perot [28], coupled with a microscope in back-scattering geometry with a x100 long working distance objective (diameter of the laser spot and its Rayleigh length are about 0.520 μm and 0.410 μm respectively), using a 532 nm Nd^{3+} :YAG laser excitation. The micro-positioning is ensured by a Marzhauser X-Y-Z motorized micro-stage with a spatial minimal step of 1 μm. Each spectrum have been recorded after a long accumulation time (about 90 minutes by spectrum), in order to obtain a good signal to noise ratio. For each data spectrum, the Brillouin shift frequency at the maximum intensity corresponds to an average of the Stokes and anti-Stokes Brillouin spectra. With the large angular aperture of the x100 objective, the minimal full width at half maximum (FWHM) of the Brillouin modes is closed to 0.5 GHz. This value had been established by measuring the FWHM of the Rayleigh Line of the laser on this polished silica substrate. For Brillouin spectrometer, several pinhole sizes are possible. To increase spatial resolution, a hole of 150 μm is selected, nevetherless this diaphragm size reduces significantly the numbers of detected photons. Then, for very small indented volumes, for example 1 N and 3 N imprints, 150 μm hole is to small to observe something. In this last context, we use a 300 μm hole.

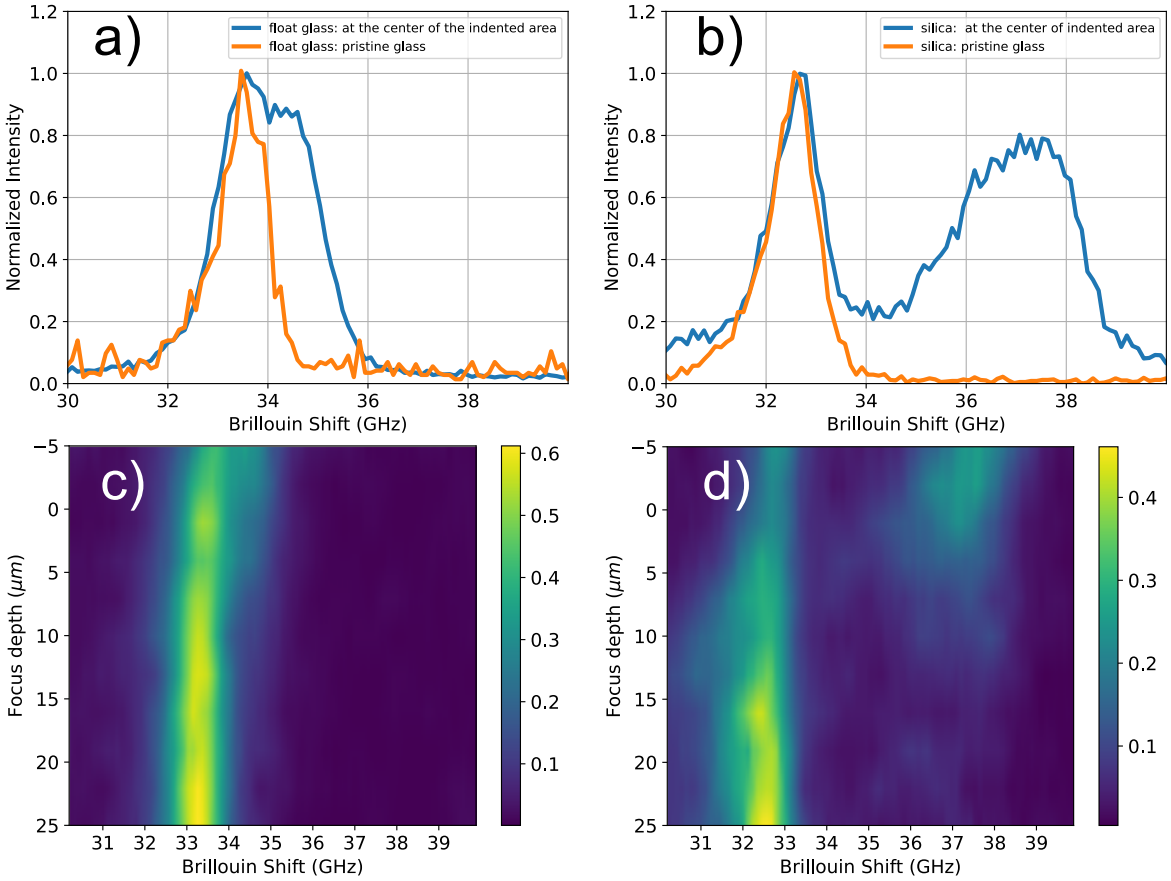

FIGURE 1: Comparison of Brillouin spectra of pristine glass and in the centre of indent of 10 N load for float glass (a) and pure silica (b) for focalisation depth equal to 0 μm (top views). Evolution of area intensity, normalized with all spectrum, of the Brillouin longitudinal acoustic mode, with depth focalisation for float glass (c) and pure silica (d). Size of spectrometer diaphragm is 300 μm

3. Results

3.1. Vertical dependance of densification for Silica and window glass imprints

Figures 1.a and 1.b show Brillouin spectra of silica and float glasses respectively for pristine glasses and at the centre of the indent surface for 10 N load. The spectrum of pristine float glass shows a well defined band, this band widens to reveal a broader band at higher frequency corresponding to the contribution of the plastically deformed region under the indent. These broadening and shift of the Brillouin line are in agreement with the previous work of Niu et al [7]. On the contrary, for silica, two distinct bands appear at the center of the indent, one corresponding to undensified silica glass and one corresponding to the contribution of highly densified glass. This last band can be attributed to the glass just below the imprint. These two distinct bands have never been seen before and needs to be understood.

The discontinuity of the Brillouin spectra, observed for silica glass and not for float glass, has to examined in the light of the nature of the optical probe used. This geometry allows us to have a high transversal resolution (in X and Y directions), but a poor vertical resolution because the laser beam is focused over length of few microns. When the laser focus is in the indented region, we observe the Brillouin spectra of the densified glasses, but also the Brillouin signal scattered by the lower layers. This second contribution is reduced due to the confocal geometry, but is still been observed [25]. In other words, the observed spectrum is mainly due to scattering within the Rayleigh region, but also from the region below and above the focused one. In order to separate the different possible contributions at different depths inside the sample, we have performed X-Y and Z scans of Brillouin measurements inside the indent. Z-Scan at the centre of the indent were obtained for both glasses by progressively varying the depth of the focus point. In order to have access to the response of the surface we performed measurements with a laser focalisation above 5 μm from the surface to 28 μm for the depth. The evolution of the normalized spectrum with depth is plotted in Figure 1.c for float glass and in Figure.1.d for silica glass. Even tough the obtained mapsare raw results, these graphs allow us to access to the depth of the indented area and its location, and to study the evolution of densification as a function of depth of focus. The results are then compared with existing models.

3.2. Evolution of Brillouin shift with radial distance for silica glass 10 N imprint.

Figure 2 shows the evolution of the Brillouin spectra with lateral positions from the centre of the indent to a distance of 15 μm along a line passing from the indent centre to a pyramid face centre at a fixed depth (depth of the imprint surface centre). We observe a large change in the Brillouin spectrum as we move away from the centre, the densified peak shifts continuously from 38 GHz to the undensified peak. The relative area of this peak is almost constant for distances less than 7.5 μm. For measurement points at distance greater than 10 μm, we observe in the Brillouin spectrum an additional component in the low energy part for the undensified peak, wich can be attributed to the scattering by glass cracks.

In order to compare the depth and lateral evolutions of the compression processes, we have plotted in Figure 3 the evolution of the position of the two peaks at the intensity maximum and their FWHM extension as a function of radial distance (3.a) and depth (3.b), for 10 N indent. The intensity of the colour, for each measurement is proportional to the relative weight of each fitted peak. As it had been demonstrated by Deschamps et al [27], from ex-situ samples recovered after irrversible high pressure experiences and using Raman and Brillouin spectroscopies, it is possible to obtain the densification ratio as a function of the maximum pressure for silica glass. Using the literal expressions of Brillouin shift and densification ratio from this last paper, we can deduce the evolution of the densification ratio in the imprint as a function of

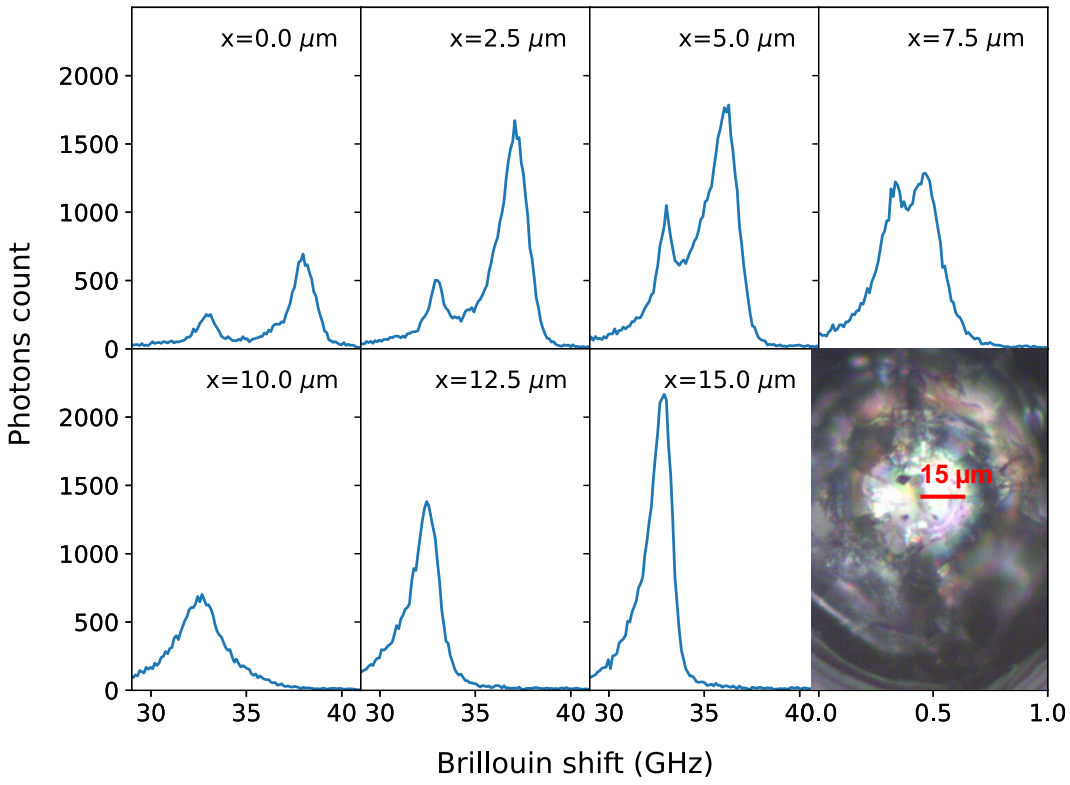

FIGURE 2: Evolution of Brillouin spectrum at z=0 μm with radial distance from the center of the indent along cross line for silica imprint obtained with a 10 N load. Size of spectrometer diaphragm is 150 μm.

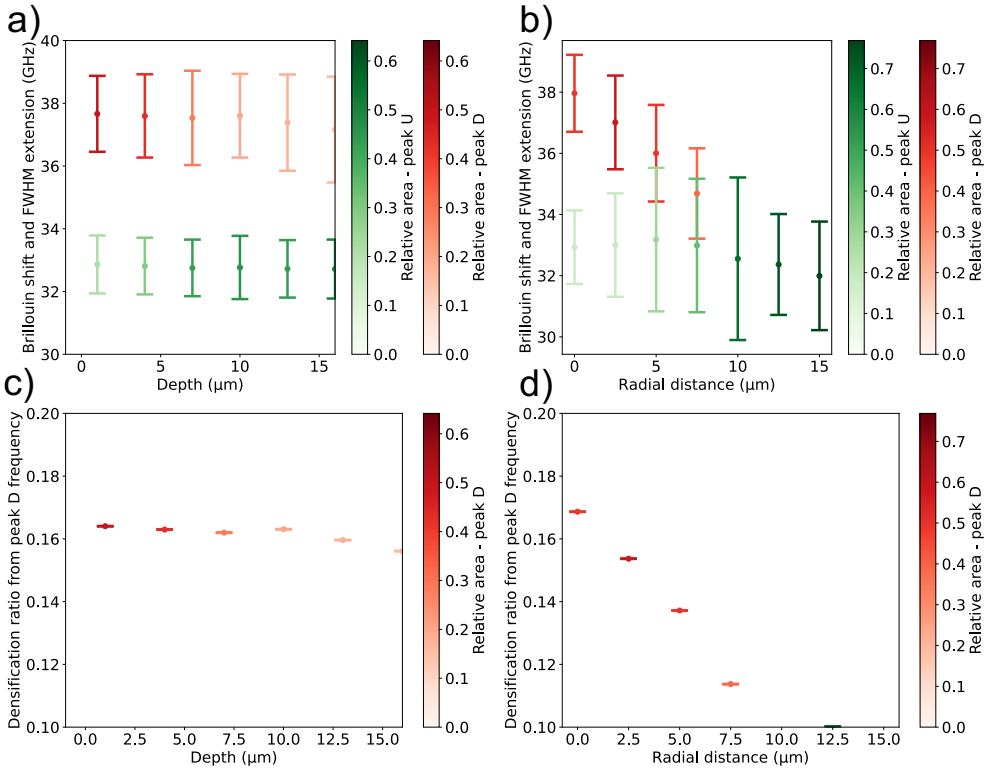

FIGURE 3: Shift and FWHM values of Brillouin longitudinal modes for the two peak, densified and undensified, as a function of radial distance (a) and depth (b). Evolution of relative intensity of densified peak with radial distance (a) and depth (b). Evolution of the densification ratio with radial distance (c) and depth (d), deduced from the densified peak frequency. Size of spectrometer diaphragm is 150 μm.

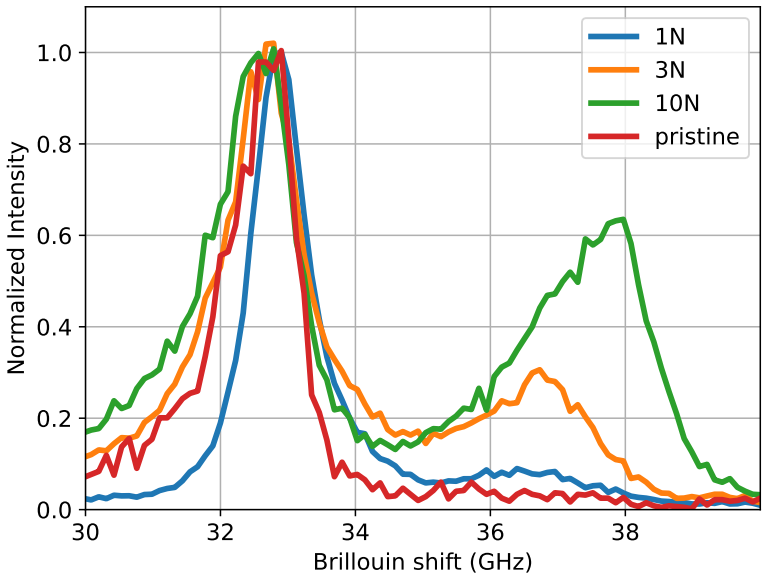

FIGURE 4: Evolution of Brillouin spectra of pristine silica glass in the centre of indent and at the surface of indent for various loads : 1N (blue curve), 3N (orange curve) and 10 N (green curve). Brillouin spectrum of non-indented silica is also plotted (red line). Size of spectrometer diaphragm is 300 μm.

radial distance and depth position. These two evolutions have been plotted in Figure.3c) and Figure.3d) respectively. We observe a very weak depth evolution of the densified peak (peak D), which never reaches the the undensified peak (peak U). As the densification process is not progressive along the depth, unlike the evolution along the radial direction. Then, in a first approach, we can question any hemispherical symmetry for the densification process.

3.3. Evolution of Brillouin shift at the imprint center with loads.

Figure 4 shows the evolution of the Brillouin spectra after indentation for different loads (from 1 N to 10 N). These spectra were measured with a laser focus at the surface of the indent centre. For comparison, the Brillouin spectrum of undensified silica has been added to the figure. The two peaks described above are observed for all loads. It appears that the position and intensity of the peak D depends on the load of the indenter. Figure 5 presents the evolution of the relative weight of peak D, as a function of the depth of focus, for the different indenter loads. The relative weight of peak D is calculated by dividing the area of peak D by the sum of the areas of each peak. These plots give access to the location of the modified area, under the imprint and its evolution with load. As expected, we observed an increase in the densified area with load indenter. Although this study is hampered by the Gaussian structure of the laser beam which is

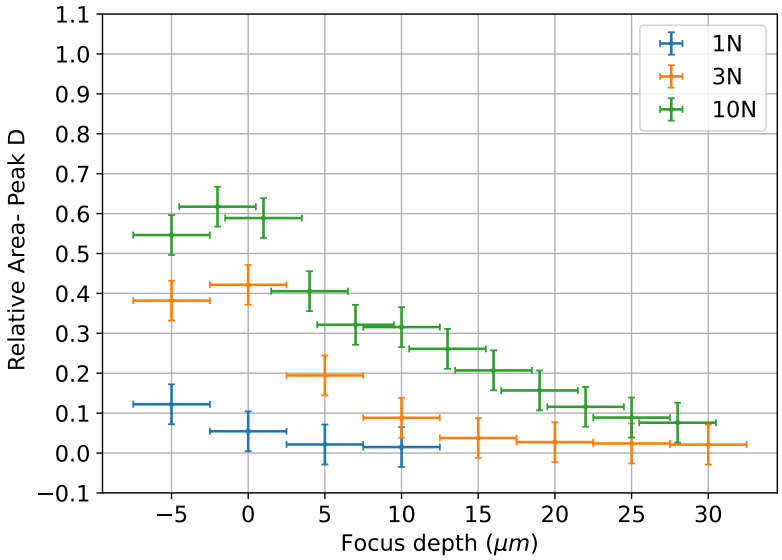

FIGURE 5: Evolution of densified peak D area divided by sum of peak U and peak D area with focalisation depth for various load : 1 N (blue curve) 3N g (orange curve) and 10 N (green curve). Size of spectrometer diaphragm is 300 μm.

focused oover a length equal to twice the Rayleigh zone, in our case just over 1 μm, it is possible to study the evolution of the densification location at the μm scale. The evolution of the Brillouin shift as a function of the depth of focus is different from 1 N to 10 N mass load. In fact, for the 1 N curve, the densified peak (peak D) is significant only at the surface of the sample (for a focus between -5 to 5 μm) and disappears just below it. Peak D is large and centred around 36.2 GHz, which means that we are already observing densified silica at this loading. From the results of Deschamps results[27], with the maximum of peak D, we can roughly estimate a densification ratio of 14% for 1 N sample for a depth equal to 0 μm. For the 3 N indented sample, the maximum of the Brillouin shift is about 36.8 GHz, corresponding to a densification of about 15 %, and is localised at the surface of the sample. For this sample, the relative area of the peak D is less than 10% for a depth of focus of 10 μm. For the 10 N sample, the densification appears to be higher, 17%, than for the 3 N sample and on a larger volume. Since the strain distribution is expected to be invariant due to the equivalent cone shape of the indenter, this variation of the maximum density with load may illustrate the difficulties of the spectroscopic mapping at small sizes.

4. Discussion

4.1. Brillouin spectrometry capacity to differentiate the undensified and densified glass answers

For float glass, as a normal glass, the densification process appears to be progressive in all directions, with a constant decreasing in densification as one moves away from the area [7]. This progressive density change has already been confirmed by Raman experiments and FE simulations [20]. Brillouin spectrometry shows a broadening and a slight shift of the line towards higher energy. Nevertheless, the Brillouin shift of the longitudinal mode have a small amplitude variation from 33.5 GHz to 34 GHz between pristine and fully densified float glass, at the limit of the resolution of the spectrometer, equal to 0. 5 GHz. Our spectrometer does not allow us to resolve a possible substructure of the Brillouin spectra. This variation is too small to conclude on the presence or the absence of a sublayer with uniform densification. Nevertheless, the well-documented theoretical and experimental results show that this progressive density change around the imprint centre perfectly matches the cracks pattern of float glass.

In the literature, the densification ratio of silica can be determined from Raman measurements using the position of the barycentre, called the centroid, of the main band [26]. Studying of the z-dependence of densification after indentation and using main band Raman spectrometry become an hazardous challenge due to the large spectral overlap of densified and undensified components [25]. This measure can, at best, propose a mean spectrum between densified region where the laser is focused and the far-field response of the undensified glass as suggested by Bruns. Our results show that Brillouin spectrometry for silica indentation has the advantage of spectrally separating the two components and allowing us to follow the evolution of densification with z. For silica, as an anomalous glass, the amplitude of densification is large enough to observe modifications of the Brillouin peak position and structure, which varies from 31.5 GHz to 38 GHz. Our Brillouin spectrometer is able to distinguish the substructure of the Brillouin spectrum produced by different densified regions (Fig.1).

As we have seen few intermediate components between the densified and undensified peaks, we can conclude that the densification does not decrease continuously from the surface of the indent. However, in Fig.3a we see a densified peak with a FWHM around 2 GHz, which is broader than the undensified peak. So we have an inhomogeneous broadening of the Brillouin line due to a partial gradient of densification within the indented area. We do not observe a fully densified silica, but an intermediate densified silica with a densification ratio varying between 14 and 16.6 %. This result suggests that the permanent densification under the indentation does not decrease smoothly with depth from the indentation point surface as it has been observed on float glass and previously in the literature on silica [21,25].

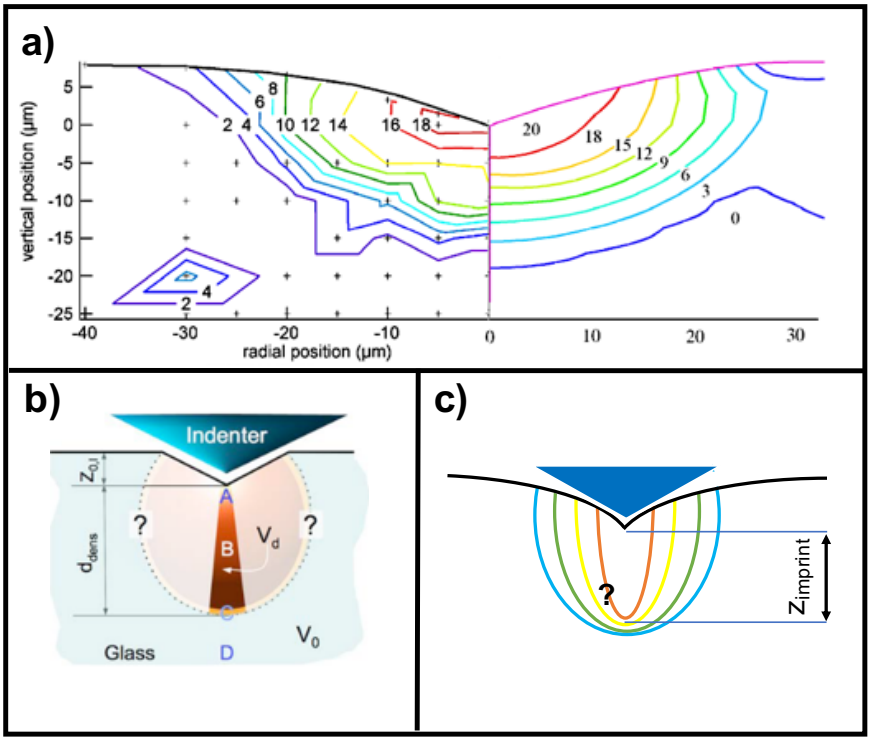

FIGURE 6: Densification profiles of indented silica glass from various experimental works.a) cross-section densification map from Raman experiments (left panel, Perriot et al [21]) and corresponding map from finite element calculation (right panel,Kermouche et al [11]) b) shematic description of density profile beneath the indenter from chemical dissolution experiments probed by AFM (Niu 2012) c) Schematic iso-density map reflection the Brillouin spectroscopy results from this present study

This vertical discontinuity in the densification process could be understood by considering the difference in compressibility and availability of each material to shear flow : silica, as an anomalous glass, is a highly compressible glass with a maximum density change of about 21% and float glass, as a normal glass, has a lower maximum density change of about 6%. As Januchta et al explains that, depending on densification ability and Poisson's ratio, two mechanical behaviours occur under indentation [29]. For sufficiently high Poisson's ratios, for example float glass with a Poisson's ratio of 0.23, which ensures a large shear flow, we observe a progressive decrease of densification in both the lateral and longitudinal directions of the imprint [7,20]. For low Poisson's ratio materials, e.g. silica glass with a Poisson's ratio equal of 0.15, the density pattern under the imprint is not clearly defined. Our results do not agree with the experimental Raman results obtained by [21] and shown in Fig.6a, where the densification is progressive along the vertical and lateral directions. In this case, these results were obtained from Raman scattering, using the evolution of the D2 shift as a function of density. However, we have recently demonstrated that the D2 line (position and intensity) is highly dependent on the thermomechanical history the densified silica [30]. Then, the reliability of a clear relations between the D2 line and density is not so obvious. Nevertheless, our present results are consistent with the FE simulation of a 2D-axisymmetric cone, where a quasi-homogenous densified region was observed, followed by a rapid decrease in densification below [21]. Rouxel et al has hyptothesised the creation of a densified region below the indented surface with a sharp transition to the far-field undensified region [17]. To our knowledge, only the experimental work of Niu et al, shown in Fig.6b), has demonstrated such behaviour for silica glass but also for soda-lime glass [24]. Our present results, resumed in scheme fig.6c), confirm and refine this "discontinuous" model along the vertical direction for silica glass : we clearly demonstrate a small thickness, dz for the transition region from densified, extending from the surface to $z_{imprint}$, to undensified glass. Niu's description and our work diverge in the lateral direction : unlike their work, we observe a progressive decrease in densification from the centre of the imprint. This last result seems to agree at least qualitatively with the predictions of Kermouche et al [11]. As a rapid decrease in density between the densified area and undensified regions induces high local stresses, it could explain the origin of the large lateral crack, under the plastic core of the indent, currently observed for silica [19].

4.2. Test of density evolution

In order to compare our experimental results with indentation simulations, we have calculated Brillouin spectra scattered by two model imprints : one in which the densification ratio evolves linearly from its saturation value (21%), the other in which the densification is constant up to a certain depth and then decreases rapidly and linearly with depth and then falls to a value close to 0. In a first approximation, we

have also assumed invariance of the the indent characteristics in the planar directions (X and Y). Since we have measured the evolution of the experimental Brillouin spectrum with focus depth, we have calculated and compared Brillouin spectra emitted by the sample for different focus depths. For the first densification model, the slope is the free parameter, for the second model, the densification ratio of the homogeneous region, the beginning and the end of the slope are free parameters.

The calculated Brillouin spectra result from the laser scattered at all depths of the sample. We assume that the number of Brillouin photons is proportional to the incident laser intensity which is calculated for each glass slice, at a distance z from the laser focus point. We have assumed that each glass slice, with a densification rate given by the densification evolution curve to be tested, produces a Brillouin spectrum with a Lorentzian profile $L(\nu - \nu_B(z))$ with a central position $\nu_B(z)$ derived from the paper of Deschamps et al densification factor-Brillouin shift calibration curve [27]. The FWHM of the Lorentzian profile was determined experimentally using a homogeneous glass plate (0.5 GHz). Before integrating the response of each layer over the entire thickness of the sample, it is necessary to consider and estimate the confocal filtering of the light for each slide of the sample.

The estimation of the confocal filtering is based on the work of Grauw et al [31] and is structured around 2 assumptions : the Gaussian structure of the scattered beam and the confocal detection. For each sample slice, located at a distance z from the focus point, we have calculated the light scattered by the slice and transmitted through the pinhole with a diameter R_{ph}. We then obtained a confocal filtering factor, $f_{R_{ph}}(z)$ for each z. This factor represents the ratio between the intensity scattered by the slice collected with the pinhole and that collected without.

We have defined r, the radius of the incident laser beam at a distance z from the laser focus point. This radius is given by

$$r(z) = r_0\sqrt{1 + (z/Z_r)^2}$$

where r_0 is the radius of the laser beam point at the focus point and Z_r the Rayleigh length of the Gaussian incident laser beam.

We have defined r' as the radius of the image with the detection system of the irradiated area in the sample located at z , z' as the image shift offset from the pinhole position. The expressions of r' and z' were calculated by conjugation relation for microscope from r and z. We have assumed that the structure of the scattered light collected by the miscroscope has a gaussian beam structure with $Z_{r_{image}}$, the Rayleigh length associated with the image gaussian beam focused at z'. To estimate the confocal filtering factor $f_{R_{ph}}(z)$, we

had to calculate $r_{at_{ph}}$ the radius of the image Gaussian beam calculated at the pinhole position :

$$r_{at_{ph}}(z) = r' \sqrt{1 + (z'(z)/Z_{r_{image}})^2}$$

Finally, rhz expression for $f_{R_{ph}}(z)$ for a slice at z from the laser focus point is :

$$f_{R_{ph}}(z) = 1 - exp(\frac{-2R_{ph}^2}{r_{at_{ph}(z)}^2})$$

Once we have obtained the evolution of $f_{R_{ph}}(z)$ with depth shift z, the total scattered Brillouin spectrum generated by sample, is obtained by integration :

$$S_{Brillouin}(\nu) = \int_{-\infty}^{+\infty} L(\nu - \nu_B(z)) \cdot f_{R_{ph}}(z) \cdot dz$$

From these expressions, we can calculate the evolution of the Brillouin spectra as a function of the laser focus depth for the two models : the "continuous" one and the "step" one and compare them with the experimental spectra.

By optimising the overlap between the experimental spectra and the modelled spectra, we have attempted to determine the best densification profile that verifies the experimental values for continuous densification ratio and "step" densification ratio evolutions. The results of these optimisations are plotted in Figure.7 for 10 N imprint. In the lower right figure, the optimised evolutions of densification fonctions for the two models are plotted. In Figure7, three experimental Brillouin spectra for different focus depths (-2 μm (a),4 μm (b), and 10 μm(c)) and the modelled spectra are shown. It appears that the step model for densification is much better at reproducing the evolution of the Brillouin Spectra than the continuous one. We can also see that our model does not reproduce well the linewidth of the densified peak D, which can be a signature of non-uniform densification in the planar direction and a lack of lateral resolution even with our x100 microscope objective, as seen in Fig.3d and by Bruns et al [25]. The best values for this step model are a maximum densification ratio equal to 16.2%, a thickness $z_{imprint}$ for the densified zone equal to 7.3 μm and a thickness dz for the transition part equal to 12.3 μm. The uncertainty in determining the thickness of the transition is about 1.5 μm. In a reasonable way, we can conclude that the progressive model in z profile is not valid, because it cannot in any way reproduce the two peaks profile and its evolution with depth that we observe experimentally. Our new experimental results therefore provide a pertinent test to challenge theoretical and simulated models of densification within the indented region.

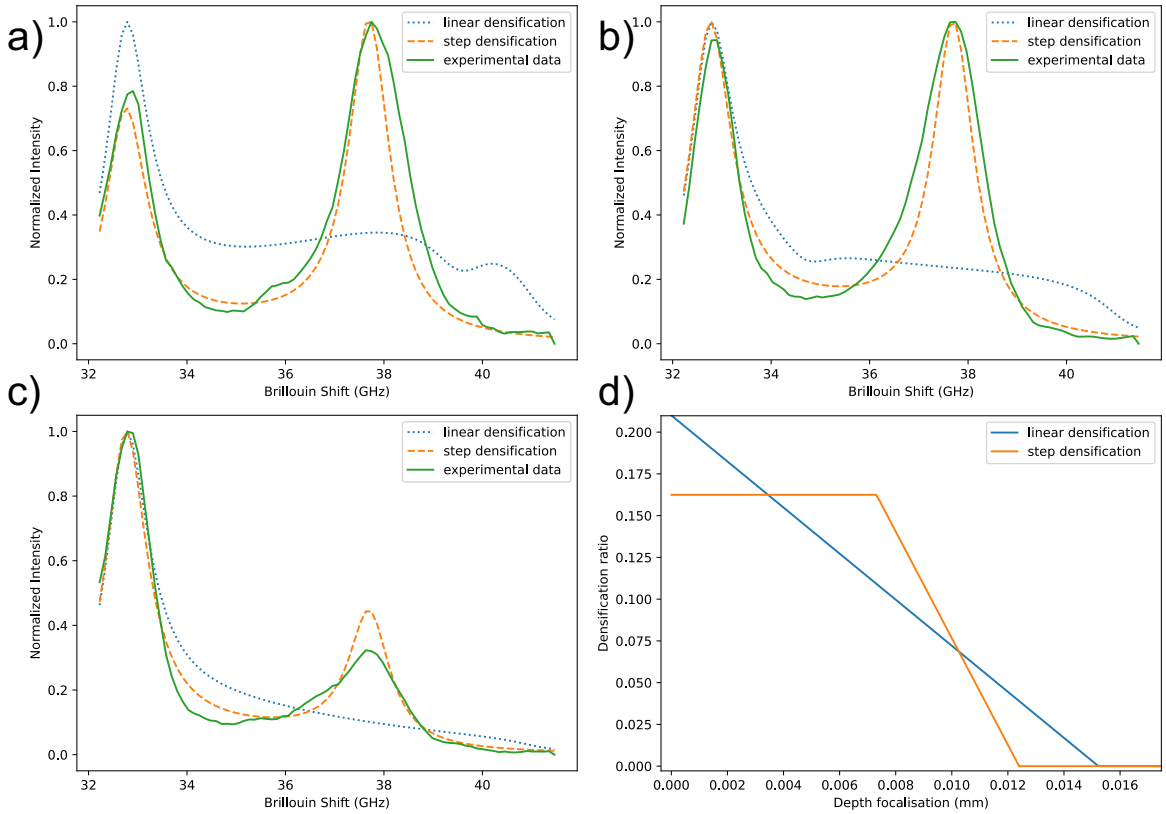

FIGURE 7: Evolution of modeled Brillouin spectra (continuous densification in blue and step densification in orange) for focus laser depth : -2 μm (a),4 μm(b) and 10 μm (c) compared to experimental data. For experimental spectra, size of spectrometer diaphragm is 150 μm.

5. Conclusion

Density mapping from micro-Brillouin scattering on micro-indentation imprints had revealed large differences between the Brillouin spectra of silica and float glass. Concerning float glass, our present results confirm a progressive density evolution but do not allow us to conclude on the presence or not of a highly densified core inside the imprint. On the contrary, the depth profile of the imprint on silica shows a quasi-homogeneous densification region whose size depends on the load, followed by a smaller transition region to undensified glass. Our experimental results have allowed us to observe and to confirm the localisation of this boundary region below the highly densified glass.A more progressive evolution of density is observed in the lateral direction. To date, and to our knowledge, no model predicts this profile of densification. Our experimental results therefore highlight the need to propose a new model for densification under indentation that explains the results observed and detailed in this paper. This work has also demonstrated the strenght of Brillouin spectrometry to refine our understanding of plastic deformation in glasses. As improving the mechanical strength of silicate glasses remains a key challenge, a step change in our understanding of the mechanisms involved is essential.

References

[1] T. Rouxel, J. Jang, U. Ramamurty, Indentation of glasses, Progress in Materials Science 121 (2021) 100834. https ://doi.org/https://doi.org/10.1016/j.pmatsci.2021.100834.

[2] R.J. Hemley, H.K. Mao, P.M. Bell, B.O. Mysen, Raman spectroscopy of siO_2 glass at high pressure, Phys. Rev. Lett. 57 (1986) 747–750. https ://doi.org/10.1103/PhysRevLett.57.747.

[3] L. Huang, J. Kieffer, Amorphous-amorphous transitions in silica glass. II. Irreversible transitions and densification limit, Phys. Rev. B 69 (2004) 224204. https ://doi.org/10.1103/PhysRevB.69.224204.

[4] B. Champagnon, C. Martinet, M. Boudeulle, D. Vouagner, C. Coussa, T. Deschamps, L. Grosvalet, High pressure elastic and plastic deformations of silica : In situ diamond anvil cell raman experiments, Journal of Non-Crystalline Solids 354 (2008) 569–573. https ://doi.org/https://doi.org/10.1016/j.jnoncrysol.2007.07.079.

[5] C.J. Benmore, E. Soignard, S.A. Amin, M. Guthrie, S.D. Shastri, P.L. Lee, J.L. Yarger, Structural and topological changes in silica glass at pressure, Phys. Rev. B 81 (2010) 054105. https ://doi.org/10.1103/PhysRevB.81.054105.

[6] T. Deschamps, C. Martinet, J.-L. Bruneel, B. Champagnon, Soda-lime silicate glass under hydrostatic pressure and indentation : A micro-raman study, Journal of Physics : Condensed Matter 23 (2011) 035402. https ://doi.org/10.1088/0953-8984/23/3/035402.

[7] H. Tran, S. Clément, R. Vialla, D. Vandembroucq, B. Rufflé, Micro-Brillouin spectroscopy mapping of the residual density field induced by Vickers indentation in a soda-lime silicate glass, Applied Physics Letters 100 (2012) 231901. https ://doi.org/10.1063/1.4725488.

[8] M. Barlet, J.-M. Delaye, T. Charpentier, M. Gennisson, D. Bonamy, T. Rouxel, C.L. Rountree, Hardness and toughness of sodium borosilicate glasses via vickers's indentations, Journal of Non-Crystalline Solids 417-418 (2015) 66–79. https ://doi.org/https://doi.org/10.1016/j.jnoncrysol.2015.02.005.

[9] R. Limbach, B.P. Rodrigues, D. MÃ¶ncke, L. Wondraczek, Elasticity, deformation and fracture of mixed fluoride phosphate glasses, Journal of Non-Crystalline Solids 430 (2015) 99–107. https ://doi.org/https://doi.org/10.1016/j.jnoncrysol.2015.09.025.

[10] T. Rouxel, H. Ji, T. Hammouda, A. Moreac, Poisson's ratio and the densification of glass under high pressure, Phys. Rev. Lett. 100 (2008) 225501. https ://doi.org/10.1103/PhysRevLett.100.225501.

[11] G. Kermouche, E. Barthel, D. Vandembroucq, Ph. Dubujet, Mechanical modelling of indentation-induced densification in amorphous silica, Acta Materialia 56 (2008) 3222–3228. https ://doi.org/https://doi.org/10.1016/j.actamat.2008.03.010.

[12] G. Kermouche, G. Guillonneau, J. Michler, J. Teisseire, E. Barthel, Perfectly plastic flow in silica glass, Acta Materialia 114 (2016) 146–153. https ://doi.org/https://doi.org/10.1016/j.actamat.2016.05.027.

[13] F.M. ERNSBERGER, Role of densification in deformation of glasses under point loading, Journal of the American Ceramic Society 51 (1968) 545–547. https ://doi.org/https://doi.org/10.1111/j.1151-2916.1968.tb13318.x.

[14] S. Yoshida, Y. Hayashi, A. Konno, T. Sugawara, Y. Miura, J. Matsuoka, Indentation induced densification of sodium borate glasses, Physics and Chemistry of Glasses - European Journal of Glass Science andTechnology Part B 50 (2009). https://www.ingentaconnect.com/content/sgt/ejgst/2009/00000050/00000001/art00016.

[15] C. Sonneville, A. Mermet, B. Champagnon, C. Martinet, J. Margueritat, D.D. Ligny, T. Deschamps, F. Balima, Progressive transformations of silica glass upon densification, The Journal of Chemical Physics 137 (2012) 124505. https ://doi.org/10.1063/1.4754601.

[16] T. Deschamps, C. Martinet, D. de Ligny, B. Champagnon, Elastic anomalous behavior of silica glass under high-pressure : In-situ raman study, Journal of Non-Crystalline Solids 355 (2009) 1095–1098. https ://doi.org/https://doi.org/10.1016/j.jnoncrysol.2009.01.045.

[17] T. Rouxel, H. Ji, J.P. Guin, F. Augereau, B. Rufflé, Indentation deformation mechanism in glass : Densification versus shear flow, Journal of Applied Physics 107 (2010) 094903. https ://doi.org/10.1063/1.3407559.

[18] J.C. Lambropoulos, T. Fang, P. D.Funkenbusch, S.D.J. andM.J Cumbo, D. Golini, Surface microroughness of optical glasses under deterministic microgrinding, Appl Opt. 35 (1996) 4448–4462. https ://doi.org/10.1364/AO.35.004448.

[19] A. Arora, D.B. Marshall, B.R. Lawn, M.V. Swain, Indentation deformation/fracture of normal and anomalous glasses, Journal of Non-Crystalline Solids 31 (1979) 415–428. https ://doi.org/https://doi.org/10.1016/0022-3093(79)90154-6.

[20] A. Kassir-Bodon, T. Deschamps, C. Martinet, B. Champagnon, J. Teisseire, G.Kermouche, Raman mapping of the indentation-induced densification of a soda-lime-silicate glass, International Journal of Applied Glass Science 3 (2012) 29–35. https ://doi.org/https://doi.org/10.1111/j.2041-1294.2012.00078.x.

[21] A. Perriot, D. Vandembroucq, E. Barthel, V. Martinez, L. Grosvalet, C. Martinet, B. Champagnon, Raman microspectroscopic characterization of amorphous silica plastic behavior, Journal of the American Ceramic Society 89 (2006) 596–601. https ://doi.org/https://doi.org/10.1111/j.1551-2916.2005.00747.x.

[22] D. Vandembroucq, T. Deschamps, C. Coussa, A. Perriot, E. Barthel, B. Champagnon, C. Martinet, Density hardening plasticity and mechanical ageing of silica glass under pressure : A raman spectroscopic study, Journal of Physics : Condensed Matter 20 (2008) 485221. https ://doi.org/10.1088/0953-8984/20/48/485221.

[23] C. Martinet, M. Heili, V. Martinez, G. Kermouche, G. Molnar, N. Shcheblanov, E. Barthel, A. Tanguy, Highlighting the impact of shear strain on the SiO2 glass structure : From experiments to atomistic simulations, Journal of Non-Crystalline Solids 533 (2020) 119898. https ://doi.org/https://doi.org/10.1016/j.jnoncrysol.2020.119898.

[24] Y.-F. Niu, K. Han, J.-P. Guin, Locally enhanced dissolution rate as a probe for nanocontact-induced densification in oxide glasses, Langmuir 28 (2012) 10733–10740. https ://doi.org/10.1021/la300972j.

[25] S. Bruns, T. Uesbeck, S. Fuhrmann, A.M. Tarrago, L. Wondraczek, D. de Ligny, K. Durst, Indentation densification of fused silica assessed by raman spectroscopy and constitutive finite element analysis, Journal of the American Ceramic Society 103 (2020) 3076–3088. https ://doi.org/https://doi.org/10.1111/jace.17024.

[26] T. Deschamps, A. Kassir-Bodon, C. Sonneville, J. Margueritat, C. Martinet, D. de Ligny, A. Mermet, B. Champagnon, Permanent densification of compressed silica glass : A raman-density calibration curve, Journal of Physics : Condensed Matter 25 (2013) 025402. https ://doi.org/10.1088/0953-8984/25/2/025402.

[27] T. Deschamps, J. Margueritat, C. Martinet, A. Mermet, B. Champagnon, Elastic moduli of permanently densified silica glasses, Scientific Reports 4 (2014). https ://doi.org/10.1038/srep07193.

[28] S.M. Lindsay, M.W. Anderson, J.R. Sandercock, Construction and alignment of a high performance multipass vernier tandem Fabry-Perot interferometer, Review of Scientific Instruments 52 (1981) 1478–1486. https ://doi.org/10.1063/1.1136479.

[29] K. Januchta, R.E. Youngman, L.R. Jensen, M.M. Smedskjaer, Indentation deformation in oxide glasses : Quantification, structural changes, and relation to cracking, Journal of Non-Crystalline Solids : X 1 (2019) 100007. https ://doi.org/10.1016/j.nocx.2018.100007.

[30] C. Martinet, A. Kassir-Bodon, T. Deschamps, A. Cornet, S.L. Floch, V. Martinez, B. Champagnon, Permanently densified SiO2 glasses : A structural approach, International Journal of Applied Glass Science 27 (2015) 5401. https ://doi.org/10.1088/0953-8984/27/32/325401 .

[31] C.J.D. Grauw, N.M. Sijtsema, C. Otto, J. Greve, Axial resolution of confocal raman microscopes : Gaussian beam theory and practice, Journal of Microscopy 188 (1997) 273–279. https ://doi.org/https://doi.org/10.1046/j.1365-2818.1997.2620818.x.